

Nanoscale

Accepted Manuscript



This is an *Accepted Manuscript*, which has been through the Royal Society of Chemistry peer review process and has been accepted for publication.

Accepted Manuscripts are published online shortly after acceptance, before technical editing, formatting and proof reading. Using this free service, authors can make their results available to the community, in citable form, before we publish the edited article. We will replace this *Accepted Manuscript* with the edited and formatted *Advance Article* as soon as it is available.

You can find more information about *Accepted Manuscripts* in the [Information for Authors](#).

Please note that technical editing may introduce minor changes to the text and/or graphics, which may alter content. The journal's standard [Terms & Conditions](#) and the [Ethical guidelines](#) still apply. In no event shall the Royal Society of Chemistry be held responsible for any errors or omissions in this *Accepted Manuscript* or any consequences arising from the use of any information it contains.

COMMUNICATION

Ionic liquid-modulated preparation of hexagonal tungsten trioxide mesocrystals for lithium-ion batteries

Cite this: DOI: 10.1039/x0xx00000x

Xiaochuan Duan, Songhua Xiao, Lingling Wang, Hui Huang, Yuan Liu, Qihong Li and Taihong Wang*

Received 00th January 2012,

Accepted 00th January 2012

DOI: 10.1039/x0xx00000x

www.rsc.org/

Hexagonal tungsten trioxide (h-WO₃) mesocrystals with biconical morphology were prepared by a facile ionic liquid-assisted hydrothermal route, and were further investigated as anode materials for lithium-ion batteries. Compared to other counterparts, the as-prepared h-WO₃ biconical mesocrystal exhibits excellent lithium insertion with good cyclability and rate capability, making it a promising candidate as anode material for high-performance lithium-ion batteries.

In the past decade, much attention has been paid to mesocrystals since first proposed by Cölfen and Antonietti, mainly owing to their unique composition structure: crystallographically oriented nanoparticle superstructures resulted from non-classical crystallization, which can be delineated by their high degree of crystallinity, porosity, and nanoparticle subunit ordered self-assembly.¹⁻⁴ Consequently, a broad range of interesting inorganic mesocrystals with various morphologies have been fabricated, in which most studies are focused on formation mechanism of mesocrystal, and less information is available concerning physical and physicochemical properties arising from these interesting mesocrystalline structures and their potential applications.⁵⁻¹² Considering that mesocrystals often display inherent and uniform porosity associated with well-defined nanoparticle orientation, mesocrystals could be exceedingly beneficial when used as electrode for lithium-ion batteries because of more prevalent and uniform pores that ease intercalation by decreasing the Li⁺ ion diffusion distance and pathways.¹³⁻²¹ However, it should be noted that attempts to fabricate the mesocrystalline electrodes are challenged due to their thermodynamically metastable feature. Usually, polymer additives are employed to temporarily stabilize the nanoparticle subunits in order to obtain highly stable mesocrystals.

Unfortunately, these polymer additives must be removed before mesocrystals can be used in further applications, often requiring complex treatments. Most importantly, the mesocrystalline electrodes may lose many of active sites as a result of surface reconstruction. Thus, it is still a great challenge to prepare mesocrystalline electrodes by a facile and environment-friendly route.²²⁻²⁴

Among various metal oxides, hexagonal tungsten trioxide (h-WO₃), is of particular interest owing to its well-known tunnel structures and has been widely investigated, especially as an intercalation host for hexagonal tungsten bronzes M_xWO₃ (M = Li⁺, Na⁺, K⁺, etc.) and a promising anode materials for lithium-ion batteries.²⁵⁻³³ It should be pointed that bulk h-WO₃ electrodes often suffer from low capacity and poor cycle performance, even in some case show electrochemically inactive. Considering that mesocrystalline modification of electrode materials has exhibited the significant improvement for high electrochemical performance,³⁴⁻³⁸ we try to apply this strategy into h-WO₃ electrodes in the present study. By a facile ionic liquid-assisted hydrothermal route, h-WO₃ electrodes with different morphologies and crystal forms, including biconical mesocrystal, rodlike single-crystal, and spherical polycrystal, are successfully prepared. Our experimental results demonstrate that the electrochemical performances vary significantly with the morphologies and crystal forms of h-WO₃ electrodes. Compared to other counterparts, the h-WO₃ biconical mesocrystals exhibit superior electrochemical properties with good cyclability and rate capability, which can be attributed to their inherent porosity associated and well-defined nanoparticle orientation. To the best of our knowledge, this is the first study to systematically investigate the morphology and crystal form effect on electrochemical activity of h-WO₃ with well-defined shapes. It is highly expected this facile synthesis of h-WO₃

mesocrystals can provide an interesting platform for further fundamental investigation into the shape-dependent electrochemical performance of mesocrystalline electrodes.

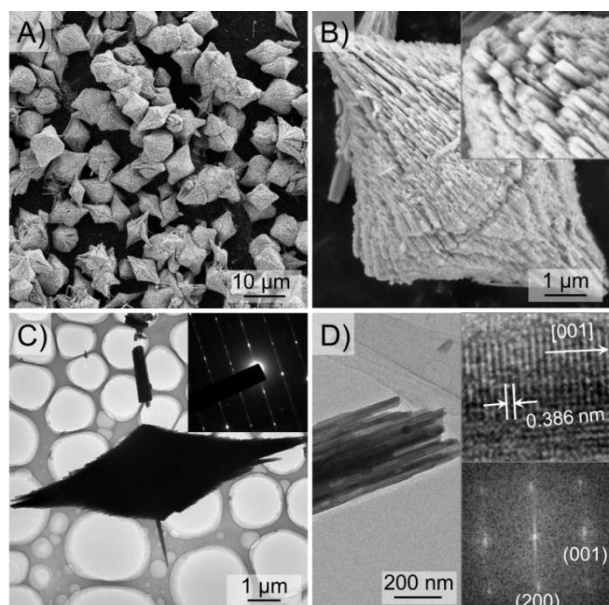


Figure 1. (A) Low- and (B) high-magnification SEM images, (C) typical TEM image and (D) corresponding HRTEM image of as-prepared h-WO₃ biconical mesocrystal, the inset of panel C is the corresponding SAED pattern.

While attempting to prepare hexagonal tungsten trioxide mesocrystals, we turned to an ionic liquid-assisted hydrothermal route using 1-*n*-butyl-3-methyl imidazolium acetate ([Bmim][CH₃COO]) as morphological control reagent (experimental details can be seen in Supporting Information). The phase and purity of the as-prepared samples were characterized by power XRD measurements, as shown in Figure S1. In all patterns, it is evident that all the diffraction peaks can be perfectly indexed to hexagonal structure of WO₃, which are consistent with the reported values (JCPDS Card 33-1387). Structurally, hexagonal WO₃ is built from chains of vertex-sharing [WO₆] octahedral, forming triangular and hexagonal tunnel structures (Figure S2). As reported,³⁹⁻⁴¹ the presence of oxalic acid and other small molecular organic acids may favour this tunnel structure of hexagonal WO₃. When we use inorganic acid, nitric acid (HNO₃) and hydrochloric acid (HCl), instead of oxalic acid in the same synthesis system, only monoclinic WO₃ nanoplates can be obtained (Figure S3 and S4). To further examine the representative morphology and structure of the as-prepared h-WO₃ biconical mesocrystal, SEM and TEM images were recorded. Figure 1A shows a typical large-area SEM image of the as-prepared sample in the presence of 5 mL of [Bmim][CH₃COO], nearly all of the samples are well-shaped microcrystal with biconical morphology. A high-magnification SEM image shown in Figure 1B reveals the obtained biconical particle surface is relatively rough and apparently built from tiny nanorods with diameters around 10-20 nm. Figure 1C shows a typical TEM image of a biconical particle, confirming that the particle consists of nanosized

subunits. The corresponding selected area electron diffraction (SAED) pattern exhibits diffraction spots indexing to [010] zone axis of hexagonal WO₃, indicating that the whole biconical particle has a single-crystal-like structure. It suggests that the whole assembly of the nanorod subunits is highly oriented, leading to the formation of the biconical particle elongated along the [001] direction. The diffraction spots are slightly elongated, indicating that there is small lattice mismatch between the nanorod subunits when they are assembled in the same orientation, which is often observed in the formation of mesocrystal.²⁰ The corresponding HRTEM image (Figure 1D) is taken at the edge of the nanorod subunit, which can be seen the clear lattice fringes. The interplanar distance is calculated as 0.386 nm, corresponding to the (001) planes of hexagonal WO₃. From the related fast Fourier transform (FFT) pattern, the diffraction spots are projected by the (001) and (200) planes and their equivalent planes under an incident electron beam along [010] axis of hexagonal WO₃, indicating the nanorod subunits are enclosed by {100} planes.

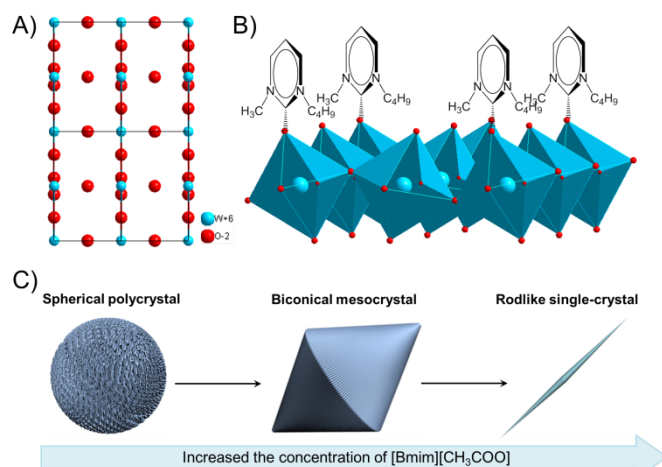


Figure 2. (A) Structure illustration of hexagonal WO₃ viewed along [100] direction; (B) Scheme for [Bmim]⁺ ions perpendicular to the {100} planes of hexagonal WO₃ and self-assemble into ordered structures along [001] direction; (C) Shape evolution of with various morphologies and crystal forms at different concentration of [Bmim][CH₃COO].

For elucidating the role played by [Bmim][CH₃COO] on the formation of biconical mesocrystal, a series of concentration-dependent experiments were conducted with other experimental conditions remain the same. In the absence of [Bmim][CH₃COO], only irregular and ill-shaped h-WO₃ spherical polycrystals with diameter ranging from 20-40 μm were produced. Compared the h-WO₃ biconical mesocrystals composed of nanorod subunits enclosed by {100} planes, an important conclusion can be drawn: the existence of [Bmim][CH₃COO] must be the key to stabilizing the {100} planes of h-WO₃ during the mesocrystal growth. On one hand, due to its good solubility and low surface tension, the introduction of ionic liquid into the synthesis system are favoured to form high supersaturation,⁴²⁻⁴⁴ which is a typical stage in the formation of mesocrystals. On the other hand, similar with mineral oxides, the surface charge on tungsten

trioxide originates from the protonation or deprotonation of surface hydroxyl groups. Both the sign and magnitude of the surface charge depend on the pH of the solution. Owing to the low point of zero charge (PZC) of tungsten trioxide (~ 0.43), the h-WO_3 particle acquired negative charges since the pH values of the present reaction medium are in the range of 1.3 \sim 2.0. Thus, the $[\text{Bmim}]^+$ ions can preferred to adsorb on the O^{2-} -terminated $\{100\}$ planes of h-WO_3 particles by electrostatic force.⁴⁵⁻⁴⁷ More importantly, the hydrogen bond, can be induced to form between the hydrogen atom at the C2 position of the imidazole ring and the bridged oxygen atoms of $\{100\}$ planes along $[001]$ direction, as shown in Figure 2. As reported, $[\text{Bmim}]^+$ ions have very strong tendency to self-assemble into ordered structures stabilized by additional π - π interactions along the aligned hydrogen bonds.⁴⁸⁻⁵⁰ Following the reason given above, $[\text{Bmim}]^+$ ions could interact strongly with the $\{100\}$ planes and align perpendicular to the h-WO_3 particles, thus promoted the preferential growth of h-WO_3 nanorod subunits exposed $\{100\}$ planes along $[001]$ direction, leading the formation of h-WO_3 biconical mesocrystal.

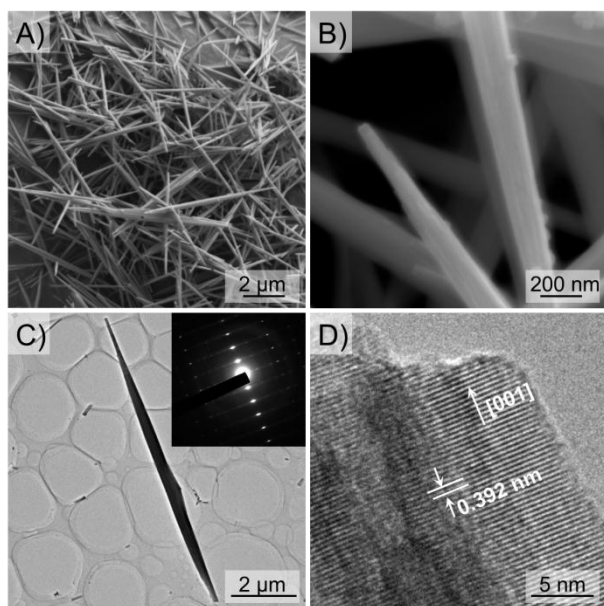


Figure 3. (A) Low- and (B) high-magnification SEM images, (C) typical TEM image and (D) corresponding HRTEM image of as-prepared h-WO_3 rodlike single-crystal, the inset of panel C is the corresponding SAED pattern.

When increased the amount of $[\text{Bmim}][\text{CH}_3\text{COO}]$ to 10 mL, h-WO_3 rodlike single-crystal were obtained (Figure 3), which can be attributed to the enhancement of stabilizing the $\{100\}$ planes in the high concentration of ionic liquid. Figure 3A shows a low-magnification SEM image, which indicates the product consists of large-scale nanorods. As shown in high-magnification SEM image (Figure 3B), the as-prepared samples are well-shaped nanorods with a diameter of 100 nm. Figure 3C depicts a typical brightfield TEM image, which shows rod morphology with a diameter of 100 nm and a length of 15 μm . The SAED pattern can be indexed to the $[010]$ zone axis of h-WO_3 , which indicates that the as-prepared h-WO_3 nanorods are

single crystals. From the corresponding HRTEM image (Figure 3F), it can be seen the clear lattice fringes and the interplane distances is calculated as 0.392 nm, corresponding to the (001) crystal planes of h-WO_3 , indicating that the nanorod exhibited a preferred growth orientation along the $[001]$ direction.

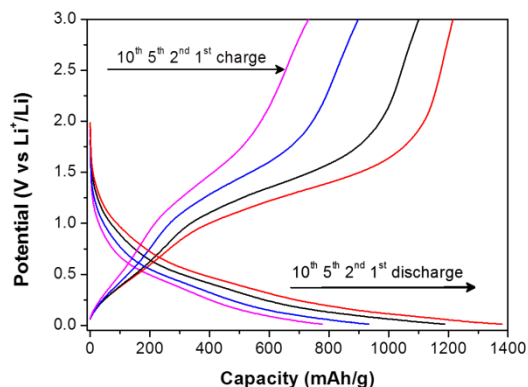


Figure 4. Galvanostatic charge-discharge profiles of h-WO_3 biconical mesocrystalline electrodes measured at 50 mA/g current density in the potential range of 0.01-3.0 vs. Li^+/Li .

There is much recent interest in h-WO_3 nanostructures as anode materials for lithium-ion batteries due to their good safety, low toxicity and large theoretical capacity (690 mAh/g). Since the as-prepared h-WO_3 samples present various morphologies and crystal forms, it gives us a good opportunity to investigate the shape-dependent electrochemical performance of h-WO_3 electrodes. To investigate the lithiation and delithiation of the h-WO_3 biconical mesocrystalline electrode, a cyclic voltammetry (CV) analysis was conducted at a scan rate of 0.1 mV/s (Figure S6). The clear cathodic/anodic peaks located at 1.43 and 0.89 V (versus Li^+/Li) are associated with lithium insertion/extraction in the lattice, which is consistent with the previous h-WO_3 report.^{25,51} Figure 4 shows the galvanostatic charge-discharge curves of the h-WO_3 biconical mesocrystalline electrode with a current density of 50 mA/g. The mesocrystalline electrode exhibits initial discharge (lithiation) and charge (delithiation) capacities of 1379 mAh/g and 1216 mAh/g, respectively. In the previous reported studies, tungsten oxide electrodes have shown noticeable capacity degradation during the initial few cycles, which greatly hindered their application for lithium-ion batteries. In the presented study, the h-WO_3 rodlike single-crystalline electrode and spherical polycrystalline electrode also exhibited capacity declines during the initial 10 cycles (Figure S7). However, the h-WO_3 mesocrystalline electrode exhibited a more stable cycling performance. The reversible capacity of h-WO_3 mesocrystalline electrode after 10 cycles was 776 mAh/g. Good cycling performance was realized over the further extended cycles (Figure 5A): 426 mAh/g was maintained after 50 cycles and the corresponding coulombic efficiency was nearly 100% at each cycle. For other counterparts, only 287 mAh/g and 222 mAh/g were maintained in the h-WO_3 rodlike single-crystals and spherical polycrystals. The improved cycle stability for h-WO_3 mesocrystalline electrode may be attributed to its

intracrystalline porosity, which can act as a buffering layer to alleviate the adverse effect of volume expansion experienced during the intercalation/de-intercalation reactions. Figure 5b presents the rate capability of the h-WO₃ electrodes with different morphologies and crystal forms from 50 to 500 mA/g for ten cycles at each current rate. It is revealed that the h-WO₃ mesocrystalline electrode retained good rate capability as the current density increased by 10 times. At low current rate (50 mA/g), the capacities of the mesocrystalline electrode and other counterparts (rodlike single-crystal and spherical polycrystal) are comparable. However, the difference increased notably as the current rate was increased. It is reasonable that the fast Li⁺ ion transport between the mesocrystalline electrode and electrolyte, where crystallographically oriented h-WO₃ nanoparticles were well connected with few grain boundaries, largely contributed to the improved lithium insertion behaviour compared with the single-crystalline electrode and polycrystalline electrode, where irregularly oriented h-WO₃ nanoparticles were connected with many grain boundaries. Therefore, our results indicate that the electrochemical properties of h-WO₃ electrodes could be significantly improved by tailoring their morphologies and crystal forms.

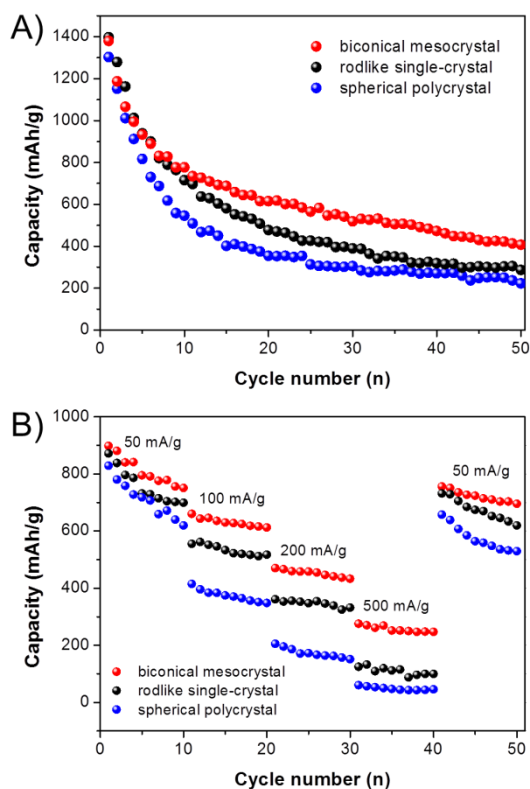


Figure 5. (A) cycling performance, and (B) rate capability of as-prepared h-WO₃ electrodes with different morphologies and crystal forms.

Conclusions

In summary, we have successfully prepared h-WO₃ mesocrystals by an ionic liquid-assisted hydrothermal route, and systematically studied the electrochemical performance as

anode materials for lithium-ion batteries. It was demonstrated that the as-prepared h-WO₃ biconical mesocrystalline electrodes exhibited improved performance compared to the rodlike single-crystalline electrode and spherical polycrystalline electrode, which could be largely attributed to the intrinsic mesocrystal nature: inherent and uniform porosity associated with well-defined nanoparticle orientation. We believe this study about the correlation between the electrochemical activity and their morphologies and crystal forms will contribute to rational design of mesocrystalline electrodes with high efficiency.

Acknowledgements

This work was partly supported by the China Postdoctoral Science Foundation funded project (Project No. 2014M560531) and the National Natural Science Foundation of China (Grant No. 61376073).

Notes and references

^a Pen-Tung Sah Institute of Micro-Nano Science and Technology, Xiamen University, Xiamen, 361000, PR China. Email: xcduan@xmu.edu.cn; thwang@xmu.edu.cn.

Electronic Supplementary Information (ESI) available: [Experimental details, XRD patterns and coulombic efficiency of the as-prepared h-WO₃ with different morphologies and crystal forms]. See DOI: 10.1039/c000000x/

- H. Cölfen and M. Antonietti, *Angew. Chem., Int. Ed.*, 2005, **44**, 5576-5591.
- J. Fang, B. Ding and H. Gleiter, *Chem. Soc. Rev.*, 2011, **40**, 5347-5360.
- R. Q. Song and H. Cölfen, *Adv. Mater.*, 2010, **22**, 1301-1330.
- M. Niederberger and H. Cölfen, *Phys. Chem. Chem. Phys.*, 2006, **8**, 3271-3287.
- H. Cölfen and M. Antonietti, *Mesocrystals and Nonclassical Crystallization*, John Wiley & Sons, Chichester, U.K., 2008.
- S. Deng, V. Tjoa, H. M. Fan, H. R. Tan, D. C. Sayle, M. Olivo, S. Mhaisalkar, J. Wei and C. H. Sow, *J. Am. Chem. Soc.*, 2012, **134**, 4905-4917.
- L. Zhou and P. O'Brien, *J. Phys. Chem. Lett.*, 2012, **3**, 620-628.
- J. S. Chen, T. Zhu, C. M. Li and X. W. Lou, *Angew. Chem., Int. Ed.*, 2011, **50**, 650-653.
- L. Zhou and P. O'Brien, *Small*, 2008, **4**, 1566-1574.
- V. M. Yuwono, N. D. Burrows, J. A. Soltis and R. L. Penn, *J. Am. Chem. Soc.*, 2010, **132**, 2163-2165.
- B. Liu and H. C. Zeng, *Chem. Mater.*, 2008, **20**, 2711-2718.
- T. Wang, H. Cölfen and M. Antonietti, *J. Am. Chem. Soc.*, 2005, **127**, 3246-3247.
- E. Uchaker and G. Cao, *Nano Today*, 2014, **9**, 499-524.
- E. Uchaker, M. Gu, N. Zhou, Y. Li, C. Wang and G. Cao, *Small*, 2013, **9**, 3880-3886.
- F. Dang, Y. Oaki, T. Hoshino, E. Hosono, H. Zhou and H. Imai, *Nanoscale*, 2013, **5**, 2352-2357.

- 16 N. Zhou, H.-Y. Wang, E. Uchaker, M. Zhang, S.-Q. Liu, Y.-N. Liu and G. Cao, *J. Power Sources*, 2013, **239**, 103-110.
- 17 N. Zhou, E. Uchaker, H. Y. Wang, M. Zhang, S. Q. Liu, Y. N. Liu, X. Wu, G. Cao and H. Li, *RSC Adv.*, 2013, **3**, 19366-19374.
- 18 Q. Li, L. Yin, Z. Li, X. Wang, Y. Qi and J. Ma, *ACS Appl. Mater. Inter.*, 2013, **5**, 10975-10984.
- 19 Z. Hong, M. Wei, T. Lan, L. Jiang and G. Cao, *Energy Environ. Sci.*, 2012, **5**, 5408-5413.
- 20 J. Ye, W. Liu, J. Cai, S. Chen, X. Zhao, H. Zhou and L. Qi, *J. Am. Chem. Soc.*, 2011, **133**, 933-940.
- 21 J. Popovic, R. Demir-Cakan, J. Tornow, M. Morcrette, D. S. Su, R. Schloegl, M. Antonietti and M.-M. Titirici, *Small*, 2011, **7**, 1127-1135.
- 22 X. Duan, L. Mei, J. Ma, Q. Li, T. Wang and W. Zheng, *Chem. Commun.*, 2012, **48**, 12204-12206.
- 23 Z. Li, P. Rabu, P. Strauch, A. Manton and A. Taubert, *Chem.–Eur. J.*, 2008, **14**, 8409-8417.
- 24 Z. Li, A. Geßner, J.-P. Richters, J. Kalden, T. Voss, C. Kübel and A. Taubert, *Adv. Mater.*, 2008, **20**, 1279-1285.
- 25 J. Lee, C. Jo, B. Park, W. Hwang, H. I. Lee, S. Yoon and J. Lee, *Nanoscale*, 2014, **6**, 10147-10155.
- 26 J. Yin, H. Cao, J. Zhang, M. Qu and Z. Zhou, *Cryst. Growth Des.*, 2013, **13**, 759-769.
- 27 L. Gao, X. Wang, Z. Xie, W. Song, L. Wang, X. Wu, F. Qu, D. Chen and G. Shen, *J. Mater. Chem. A*, 2013, **1**, 7167-7173.
- 28 C. M. Sim, Y. J. Hong and Y. C. Kang, *ChemSusChem*, 2013, **6**, 1320-1325.
- 29 J. Yang, L. Jiao, Q. Zhao, Q. Wang, H. Gao, Q. Huan, W. Zheng, Y. Wang and H. Yuan, *J. Mater. Chem.*, 2012, **22**, 3699-3701.
- 30 Y. Qiu, G.-L. Xu, Q. Kuang, S.-G. Sun and S. Yang, *Nano Res.*, 2012, **5**, 826-832.
- 31 S. Yoon, C. Jo, S. Y. Noh, C. W. Lee, J. H. Song and J. Lee, *Phys. Chem. Chem. Phys.*, 2011, **13**, 11060-11066.
- 32 K. Huang, Q. Pan, F. Yang, S. Ni, X. Wei and D. He, *J. Phys. D: Appl. Phys.*, 2008, **41**, 155417.
- 33 Z. J. Gu, H. Q. Li, T. Y. Zhai, W. S. Yang, Y. Y. Xia, Y. Ma and J. N. Yao, *J. Solid State Chem.*, 2007, **180**, 98.
- 34 D. Wang, J. Sun, X. Cao, Y. Zhu, Q. Wang, G. Wang, Y. Han, G. Lu, G. Pang and S. Feng, *J. Mater. Chem. A*, 2013, **1**, 8653-8657.
- 35 X. T. Chang, S. B. Sun, Z. J. Li, X. A. Xu and Y. Y. Qiu, *Appl. Surf. Sci.*, 2011, **257**, 5726-5730.
- 36 D. Wang, J. Li, X. Cao, G. S. Pang and S. H. Feng, *Chem. Commun.*, 2010, **46**, 7718-7720.
- 37 J. Zhang, J. P. Tu, X. H. Xia, X. L. Wang and C. D. Gu, *J. Mater. Chem.*, 2011, **21**, 5492-5498.
- 38 J. Z. Ou, S. Balendhran, M. R. Field, D. G. McCulloch, A. S. Zoofakar, R. A. Rani, S. Zhuikov, A. P. O'Mullane and K. Kalantar-zadeh, *Nanoscale*, 2012, **4**, 5980-5988.
- 39 J. Su, X. Feng, J. D. Sloppy, L. Guo and C. A. Grimes, *Nano Lett.*, 2011, **11**, 203-208.
- 40 M. Shibuya and M. Miyauchi, *Adv. Mater.*, 2009, **21**, 1373-1376.
- 41 Z. J. Gu, T. Y. Zhai, B. F. Gao, X. H. Sheng, Y. B. Wang, H. B. Fu, Y. Ma and J. N. Yao, *J. Phys. Chem. B*, 2006, **110**, 23829-23836.
- 42 X. Duan, J. Ma, J. Lian and W. Zheng, *CrystEngComm*, 2014, **16**, 2550-2559.
- 43 Z. Ma, J. Yu and S. Dai, *Adv. Mater.*, 2010, **22**, 261-285.
- 44 A. Tauber and Z. Li, *Dalton Trans.*, 2007, 723-727.
- 45 G. Zhou, X. Duan, B. Liu, Q. Li and T. Wang, *Nanoscale*, 2014, **6**, 11041-11045.
- 46 X. Duan, D. Li, H. Zhang, J. Ma and W. Zheng, *Chem.–Eur. J.*, 2013, **19**, 7231-7242.
- 47 X. Duan, T. Kim, D. Li, J. Ma and W. Zheng, *Chem.–Eur. J.*, 2013, **19**, 5924-5937.
- 48 W. Zheng, X. Liu, Z. Yan and L. Zhu, *ACS Nano*, 2009, **3**, 115-122.
- 49 Y. Zhou, J. H. Schattka and M. Antonietti, *Nano Lett.*, 2004, **4**, 477-481.
- 50 M. Antonietti, D. Kuang, B. Smarsly and Y. Zhou, *Angew. Chem., Int. Ed.*, 2004, **43**, 4988-4992.
- 51 W. Li and Z. Fu, *Appl. Surf. Sci.*, 2010, **256**, 2447-2452.